Naval Research Laboratory

Washington, DC 20375-5000

NRL Report 9303

Impulse Arrays

C. L. TEMES

Search Radar Branch
Radar Division

May 3, 1991

REPORT DOCUMENTATION PAGE

Form Approved
OMB No 0704-0188

1. AGENCY USE ONLY (Leave blank)	2. REPORT DATE	3. REPORT TYPE AND DATES COVERED
	May 3, 1991	Interim

4. TITLE AND SUBTITLE

Impulse Arrays

5. FUNDING NUMBERS

PE 62712N
RR12-132-000

6. AUTHOR(S)

C. L. Temes

7. PERFORMING ORGANIZATION NAME(S) AND ADDRESS(ES)

Naval Research Laboratory
Washington, DC 20375-5000

8. PERFORMING ORGANIZATION REPORT NUMBER

NRL Report 9303

9. SPONSORING/MONITORING AGENCY NAME(S) AND ADDRESS(ES)

Office of Chief of Naval Research
Arlington, VA 22217-5000

10. SPONSORING/MONITORING AGENCY REPORT NUMBER

11. SUPPLEMENTARY NOTES

12a. DISTRIBUTION/AVAILABILITY STATEMENT

Approved for public release; distribution unlimited.

12b. DISTRIBUTION CODE

13. ABSTRACT *(Maximum 200 words)*

This report considers impulse radar signals in terms of their propagation from an array of elements. The far-field electric vector is proportional to the derivative of the current in an infinitesimal dipole representing each element. Although not physically relizable, this model is used as an approximation to illustrate some array properties peculiar to impulse, or ultra-wideband (UWB), excitations. Thus, for example, a 1-ns rounded baseband pulse with a $\cos^2$ shape theoretically propagates as a single sinusoidal cycle centered at L-band (1 GHz) with 100% bandwidth. The far field from an array of elements is considered as a function of angle.

14. SUBJECT TERMS

Impulse radar Ultra-wideband radar
Impulse arrays

15. NUMBER OF PAGES

33

16. PRICE CODE

17. SECURITY CLASSIFICATION OF REPORT	18. SECURITY CLASSIFICATION OF THIS PAGE	19. SECURITY CLASSIFICATION OF ABSTRACT	20. LIMITATION OF ABSTRACT
UNCLASSIFIED	UNCLASSIFIED	UNCLASSIFIED	UL

CONTENTS

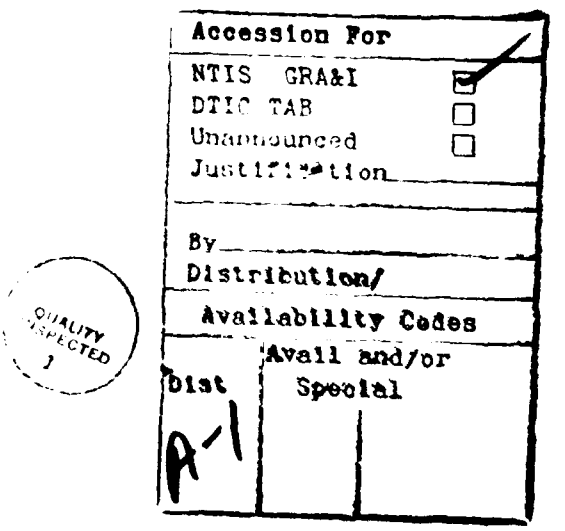

IMPULSE ARRAYS

1. INTRODUCTION

The concept of baseband radar and/or communications has existed in the literature and in practice for many years. This involves the idea of using a switch, spark gap, or other related device in a dc circuit as the energy source and propagating a signal into space.

At first look, one may be tempted to say that baseband (i.e., dc) pulses cannot be efficiently coupled to space and propagated. Yet we know of a number of examples where baseband signals cause propagation, such as:

- ignition noise
- lightning
- the original Hertz propagation experiments with spark gaps for transmission and reception
- electromagnetic pulses (EMP)
- ground-penetration radars [1]
- Rome Air Development Center (RADC) spark-gap radar experiments [2], 1968-1974
- propagation with conical antennas [3,4]
- Norfolk Ship Systems, Inc./Sperry experiments [5,6,7].

Although the subject has been in the literature for quite some time, interest has been renewed because of the development in recent years of solid state switching techniques that have the potential for generating, at baseband, very narrow pulse widths at high peak powers. Although the per-pulse energies may not be large, substantial energy for detection may be obtained by using these devices in an array and (coherently) integrating a number of pulses.

This report postulates some simple properties for a linear array of elements generating narrow baseband pulses.

2. A SINGLE ARRAY ELEMENT

2.1 In Free Space

Figure 1 shows a single hypothetical array element in free space consisting of a classical differential antenna, i.e., a small current element [8].

A time-dependent current density $\vec{J}\ (\vec{r}_o,\ t)$ in a volume V_o generates an electric vector at a remote location $\vec{r} - \vec{r}_o$ given by

$$\vec{A}(\vec{r},\ t) = \frac{1}{4\pi} \int_{V_o} \frac{\vec{J}(\vec{r} - \vec{r}_o,\ t*)}{\vec{r} - \vec{r}_o}\, dV_o\ , \tag{1}$$

Manuscript approved October 3, 1990.

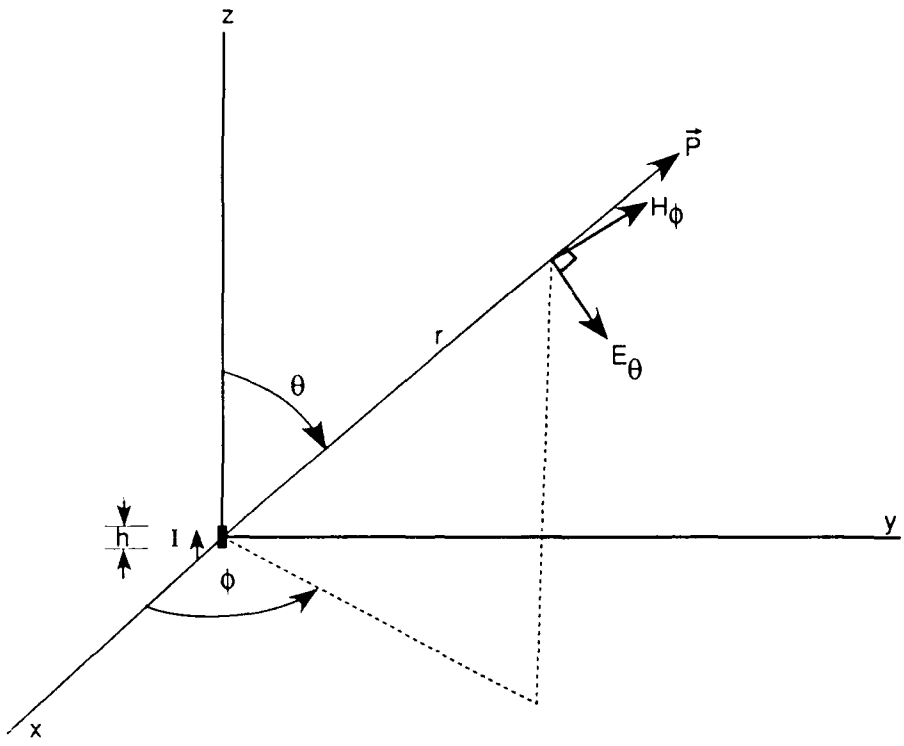

Fig. 1 — Elemental current dipole in free space

where

t^* is $t-(r-r_o)/c$.

For the elemental dipole in Fig. 1 oriented along the z axis, Eq. (1) becomes

$$\vec{A}(\vec{r}, t) = \frac{h\ I(t*)}{4\pi r}\ \hat{z}\ , \tag{2}$$

where

$I(t^*)$ is current in dipole
h is length of dipole.

The electric vector in the far field is given by:

$$\vec{E}\ (\vec{r}, t) = -\mu\ \frac{\partial \vec{A}(\vec{r}, t)}{\partial t} = \frac{-\mu h\ \dot{I}(t*)}{4\pi r}\ \hat{z}\ . \tag{3}$$

The electric field is explicitly dependent on current waveshape.

Thus, if the current is written in the form

$$I(t) = I_o\ f(t)\ , \tag{4}$$

where

I_o is constant magnitude factor
$f(t)$ is unit-amplitude waveform factor,

then Eq. (3) becomes

$$\vec{E}\,(\vec{r},\,t) = \frac{-\mu h\, I_o}{4\pi r}\,\dot{f}\,(t*)\,\hat{z}\,. \tag{5}$$

In the far field, the propagating component is E_θ, given by

$$E_\theta = \frac{\mu h I_o}{4\pi r}\,\sin\theta\,\dot{f}\,(t*)\,, \tag{6}$$

and the corresponding propagating magnetic vector component is

$$H_\phi = \frac{E_\theta}{\eta}\,, \tag{7}$$

where

$\eta = \sqrt{\frac{\mu}{\epsilon}}$, which is the intrinsic impedance of free space.

As an example, consider a current waveform consisting of a $\cos^2$ shape that is equivalent to a full cosine on a pedestal (Fig. 2(a)):

$$\begin{aligned} f(t) &= 1/2\,\left[1 + \cos\left[\frac{2\pi t}{\tau}\right]\right],\ |t| \le \frac{\tau}{2} \\ &= 0,\ |t| > \frac{\tau}{2}. \end{aligned} \tag{8}$$

In this case, the remote electric field from Eq. (6) is of the form:

$$E_\theta = \frac{-\mu h\, I_o}{4\pi r}\,\sin\theta \cdot \frac{\pi}{\tau}\,\sin\left[\frac{2\pi t}{\tau}\right],\ |t| \le \frac{\tau}{2}\,. \tag{9}$$

Figure 2(b) shows that this is a single sinusoidal cycle. For example, if the original pulse width is τ = 1 ns, the propagated wave has a carrier frequency centered at 1 GHz (L-band) with 100% 3-dB bandwidth,

$$B = \frac{1}{\tau}\,. \tag{10}$$

Figure 3(a) shows another interesting current waveform — a physically realizable square wave having rounded rise and fall times. Theoretically, disconnected positive and negative pulses occur in the far field as shown in Fig. 3(b), although waveform energy has been considerably reduced.

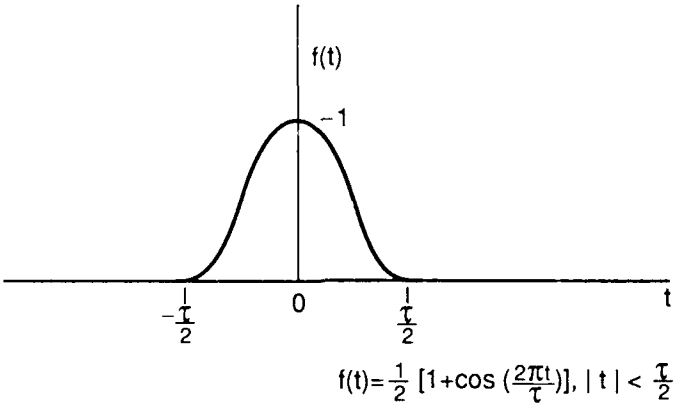

(a) Full-cosine current at source

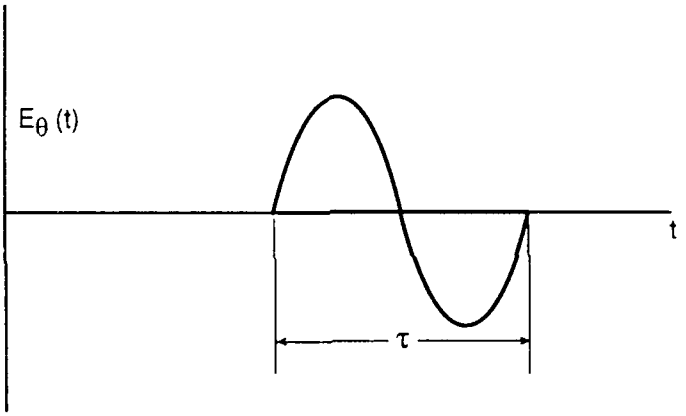

(b) Waveform at remote distance

Fig. 2 — Waveform at remote distance resulting from a full-cosine current pulse at source

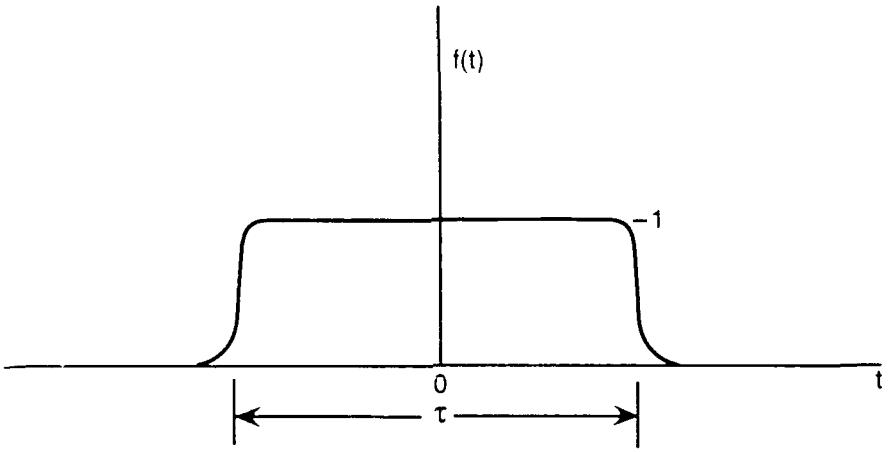

(a) Physically realizable square-wave current source

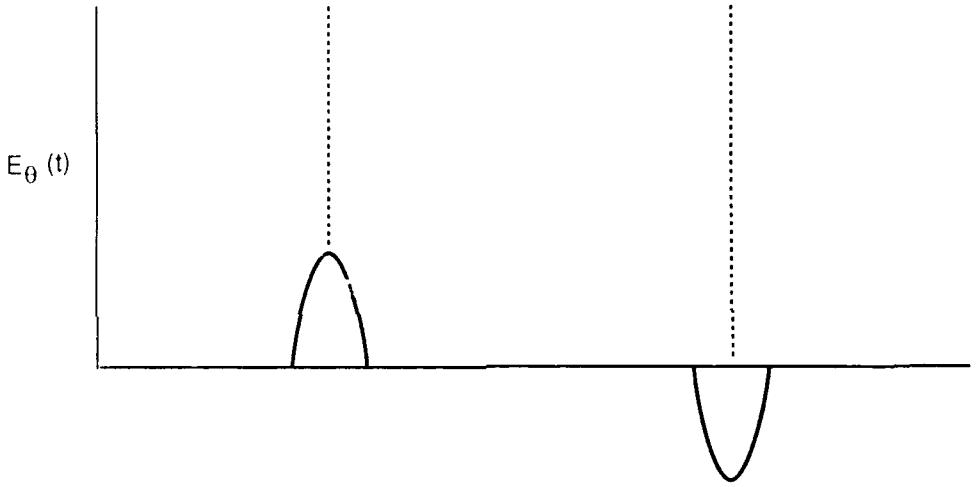

(b) Waveform at remote distance

Fig. 3 — Waveform at remote distance resulting from a physically realizable square-wave current source

2.2 With a Reflecting Back Plane

In Section 2.1, we considered an elemental dipole in free space and described some waveshapes that current pulses produce at a remote distance.

The elemental dipole, however, radiated isotropically with respect to ϕ. Figure 4 shows a more practical configuration consisting of an elemental dipole in front of a reflecting plane.* By placing the current element at a distance ℓ in front of the plane,where

$$\ell > \frac{c\tau}{2}\,, \tag{11}$$

*The reflecting back plane can be replaced by an inverted dipole image for analytical purposes, as depicted in Fig. 4.

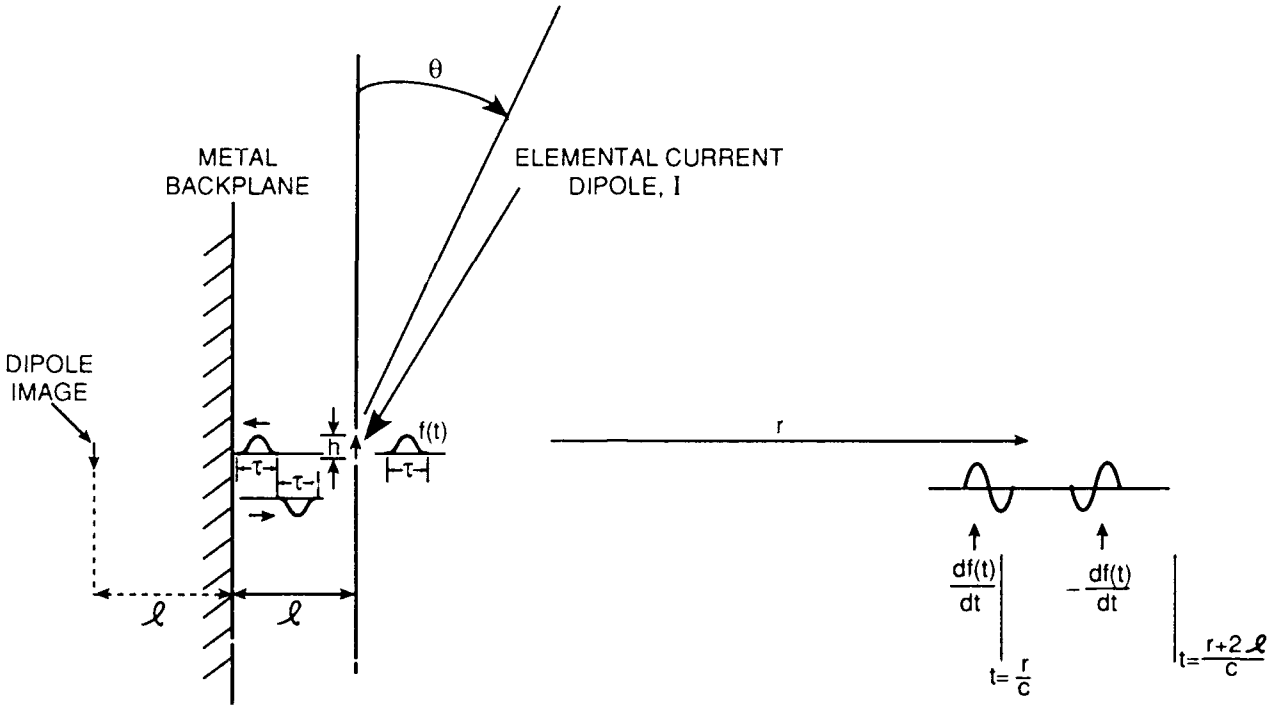

Fig. 4 — Radiation from an array element with reflecting back plane

we can ensure that no interaction occurs between the generated pulse and the reflected pulse. At the exact condition

$$\ell = \frac{c\tau}{2} , \tag{12}$$

the full cosine-on-a-pedestal current pulse, shown in Fig. 5(a), leads to the irregular waveform at a remote distance shown in Fig. 5(b). One might be tempted to let the reflected pulse be delayed by $\tau/2$ instead of τ in this case so that the negative portions of the sinusoids overlap and reinforce each other. In this case

$$\ell = \frac{c\tau}{4} . \tag{13}$$

Another option is to use

$$\ell = \frac{3\tau}{4} , \tag{14}$$

with a cosine-on-a-pedestal pulse.

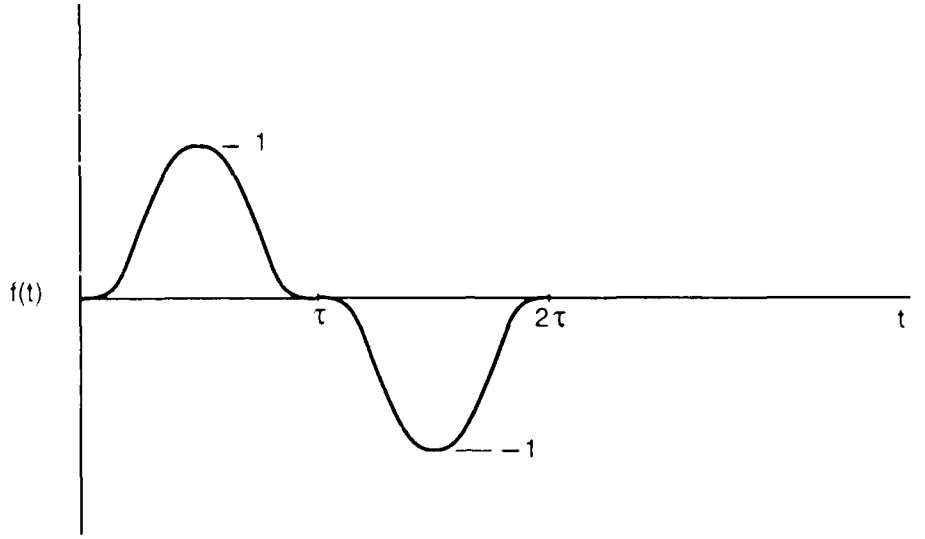

(a) Generated pulse (full-cosine-on-a-pedestal) followed by inverted reflected pulse

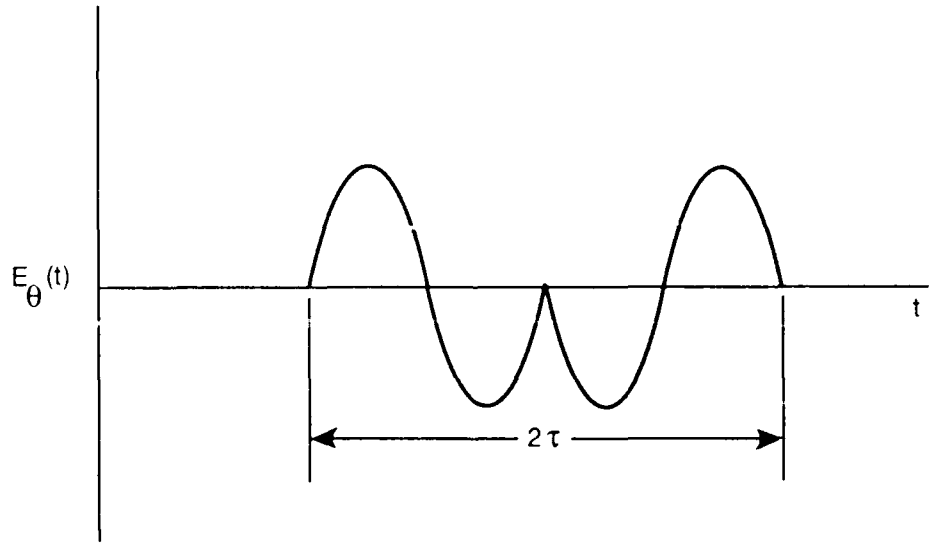

(b) Waveform at a remote distance

Fig. 5 — Waveshapes in the presence of a reflecting back plane for a full-cosine-on-a-pedestal current pulse, $2\ell/c = \tau$

Figure 6 shows the waveshapes of the latter case. At a remote distance, the waveform shown in Fig. 6(b) is at least coherent, although one half of a sinusoidal cycle is missing.

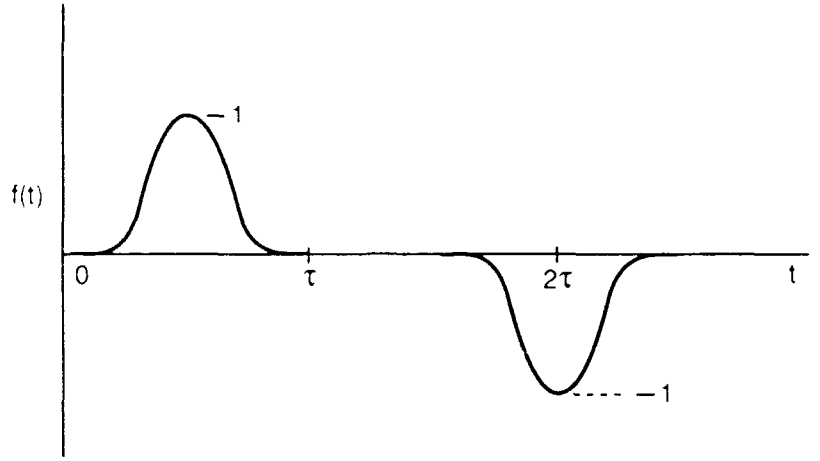

(a) Generated pulse (full-cosine-on-a-pedestal) followed by inverted reflected pulse

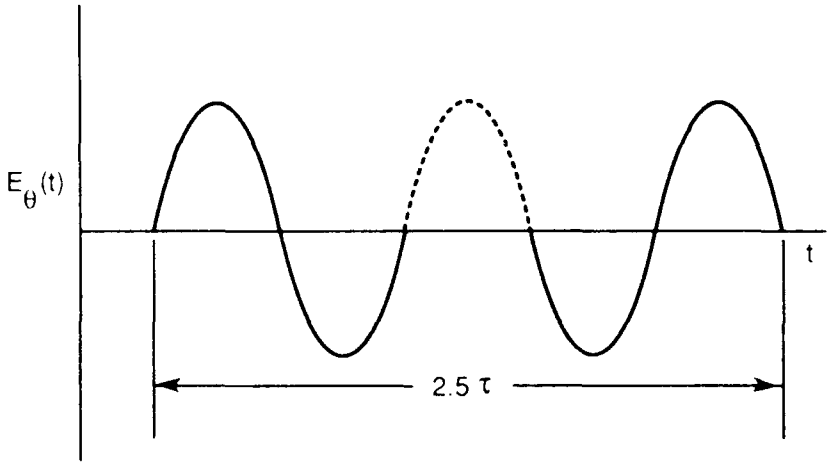

(b) Waveform at a remote distance

Fig. 6 — Waveshapes in the presence of a reflecting back plane for a full-cosine-on-a-pedestal current pulse, $2\ell/c = 1.5\tau$

2.3 With an Absorbing Back Plane

If an effective back plane absorber can be provided, the free-space results of Section 2.1 should apply for the half-space in front of the absorber.

Figure 7 summarizes the current source and long-range (derivative) waveforms for several cases, with and without a reflecting back plane.

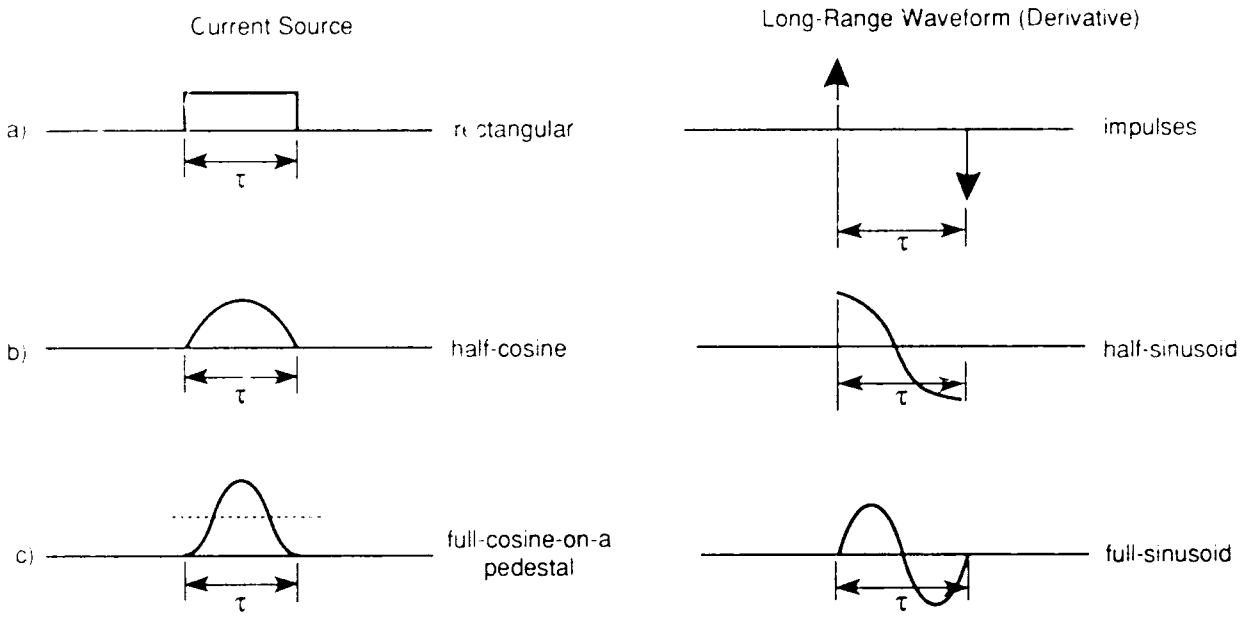

(a) In free space or with absorbing back plane

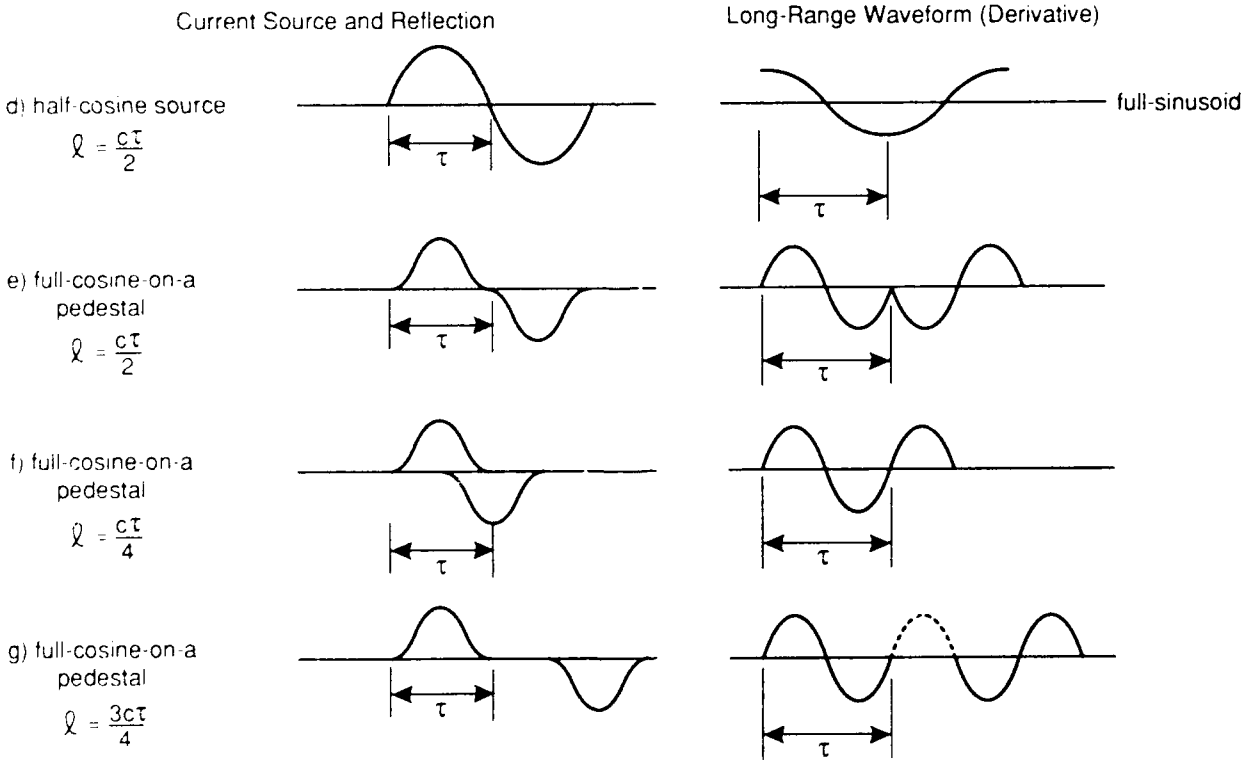

(b) With reflecting back plane at distance ℓ

Fig. 7 — Waveform summary

3. AN ARRAY OF ELEMENTS

3.1 In Free Space

Figure 8 shows an illustrative linear array of elemental current dipoles, similar to that of Fig. 1, lined up along the y axis. The dipoles are aligned parallel with the z axis, as in Fig. 1.

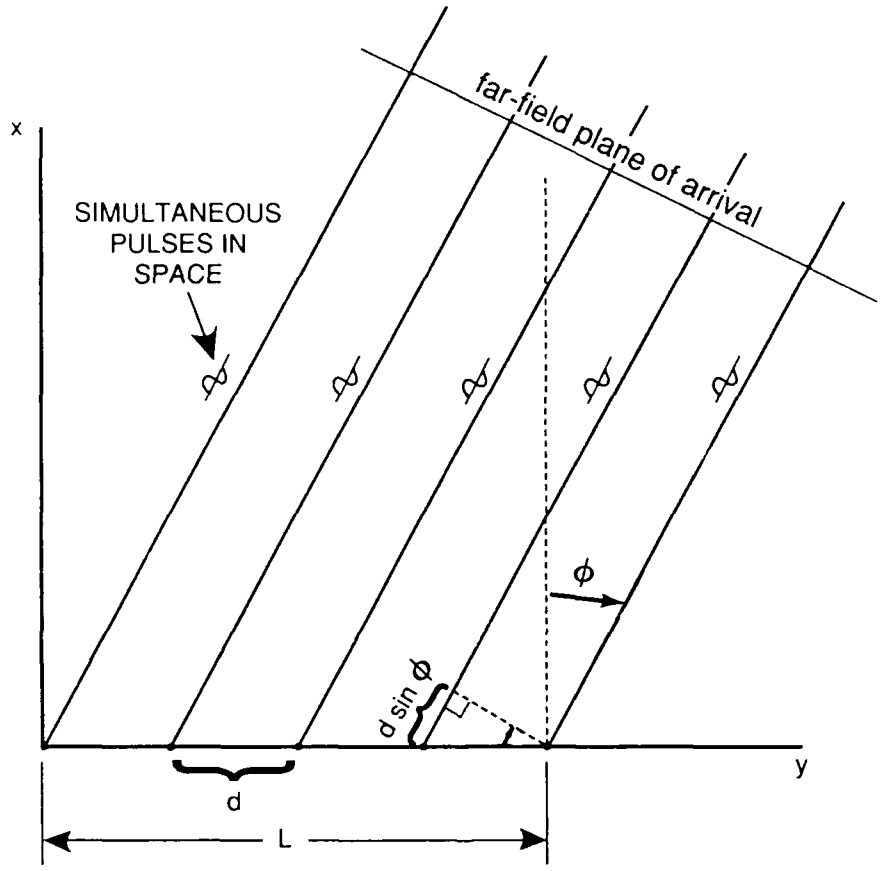

Fig. 8 — Array geometry

Let $I(t)$ be simultaneous in each of the dipoles. At a point (r, θ, ϕ), far from the origin, we have, from the center (zeroth) element,

$$A_z(t) = \frac{hI\left(t - \frac{r}{c}\right)}{4\pi r} . \tag{15}$$

From Eqs. (12) and (7),

$$E_\theta = \frac{\mu h \dot{I}\left(t - \frac{r}{c}\right)}{4\pi r} \sin\theta . \tag{16}$$

For N elements spaced at an interval d, the net electric field at the far point (r, θ, ϕ) is

$$E(t) = \frac{\mu h}{4\pi r} \sin\theta \sum_{n=0}^{n-1} \dot{I}\left(t - \frac{r}{c} + \frac{n\, d \sin\phi}{c}\right). \tag{17}$$

While conventional arrays have phase relationships between sinusoids, this system explicitly involves delayed time relationships between narrow pulses. Figure 9 shows how unit-amplitude far-field rectangular E-field pulses of width τ spread out as a function of angle off broadside for a five-element array with interelement spacing $d/c\tau = .5$. It was previously seen that far-field pulses have zero dc value, so the rectangular shape is not physically realizable. It is used here merely for illustration and may represent half of a square wave generated in the far field by a triangular current pulse or, more loosely, one of the half-cycles of a full sinusoid (to be considered later in more detail). The horizontal scale in Fig. 9 is normalized time, t/τ. Similar plots are given in Figs. 10 through 12 for $d/c\tau = 1.5$ and 2, respectively.

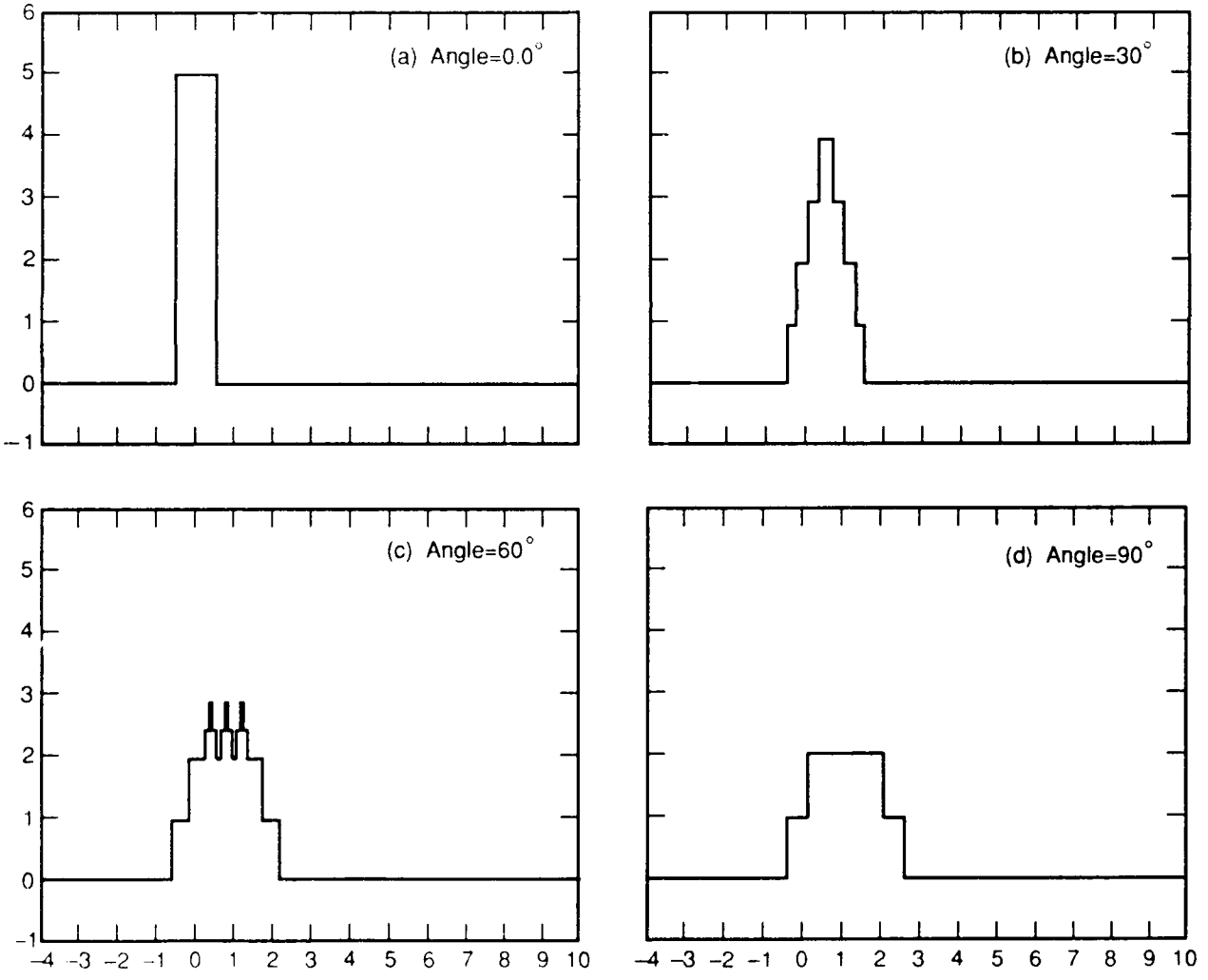

Fig. 9 — Spread of rectangular pulses, $d/c\tau = .5$

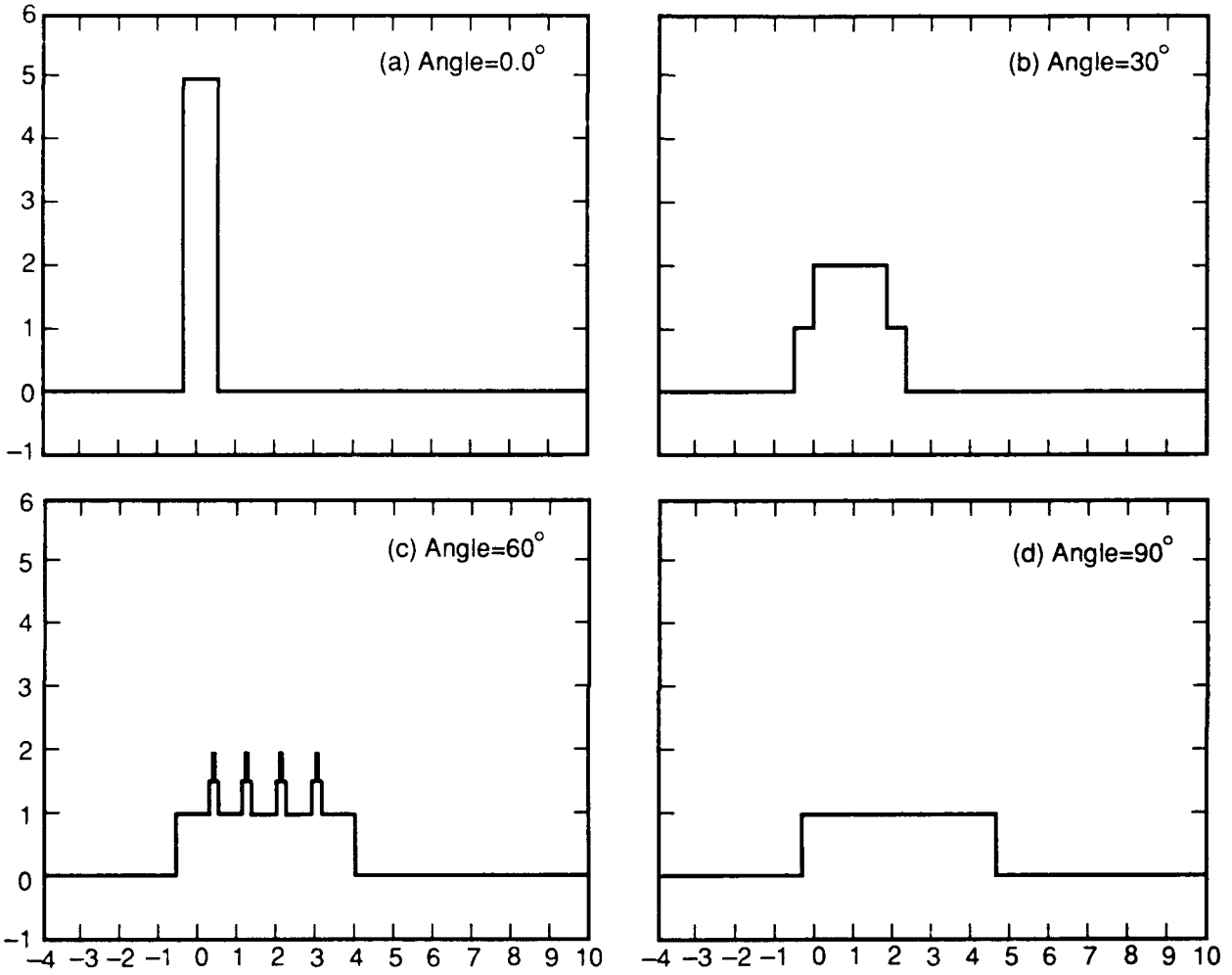

Fig. 10 — Spread of rectangular pulses, $d/c\tau = 1$

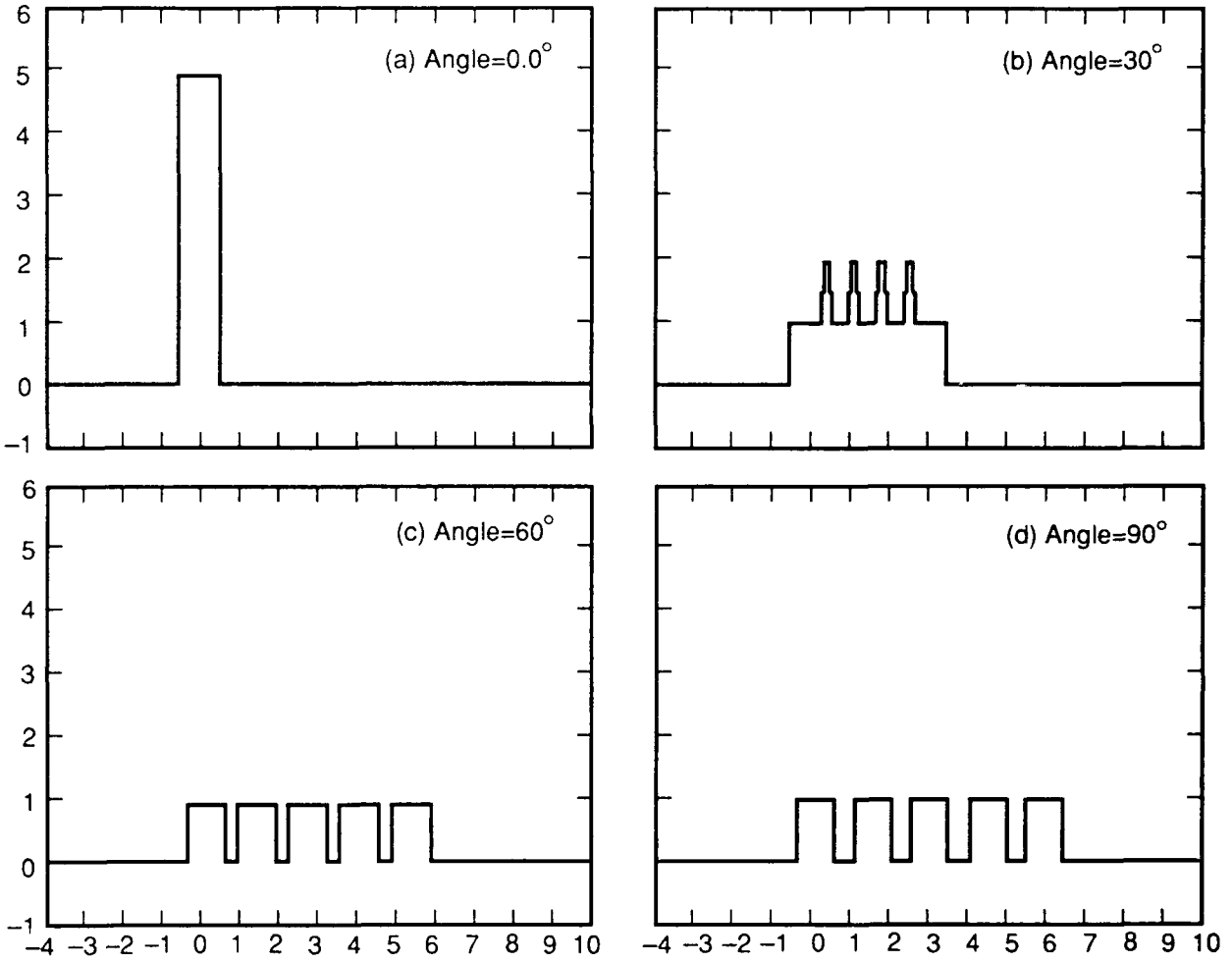

Fig. 11 — Spread of rectangular pulses, $d/c\tau = 1.5$

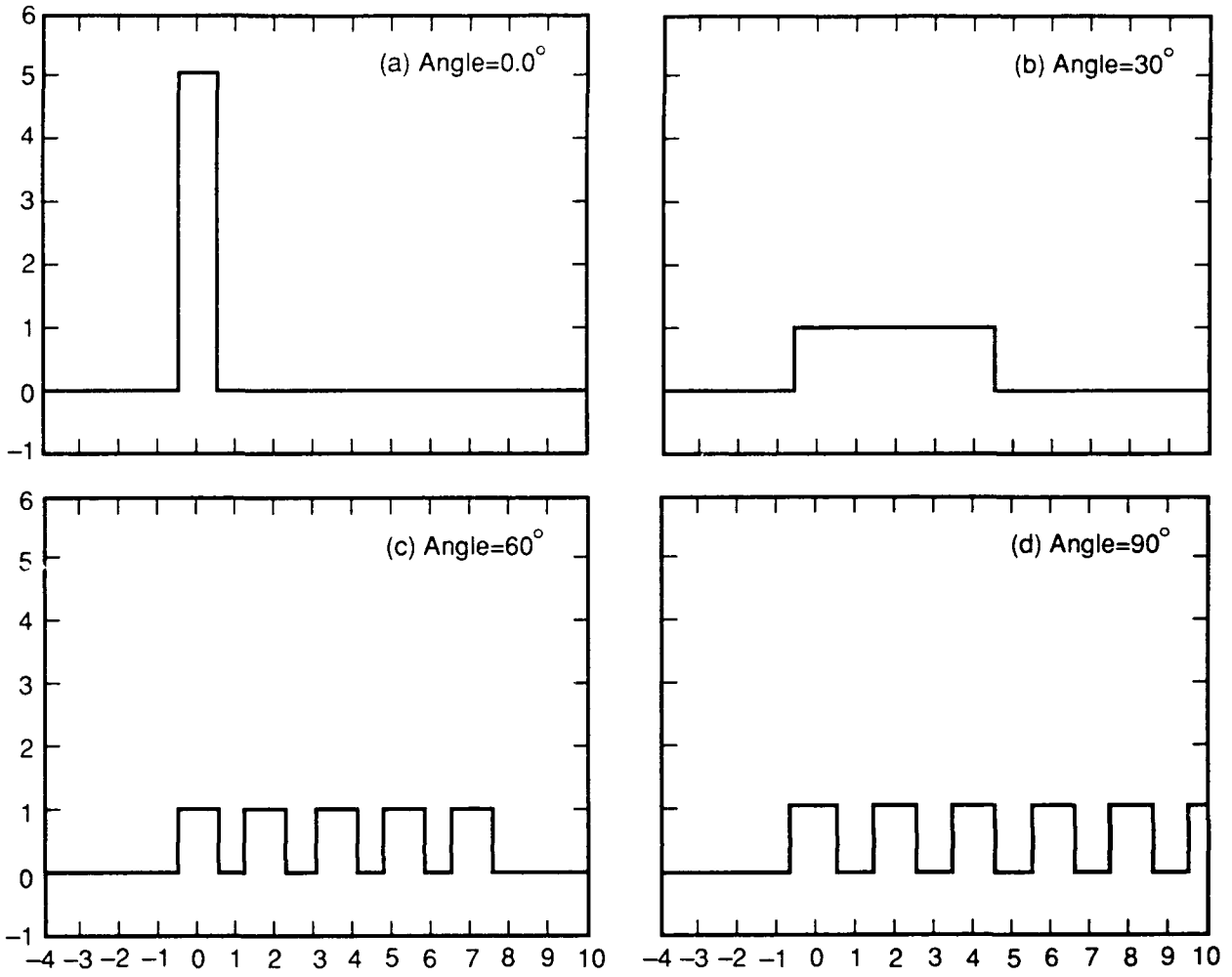

Fig. 12 — Spread of rectangular pulses, $d/c\tau = 2$

3.2 Beamwidth

Voltage/Power Definition

Starting from $\phi = 0$, as we move to the right in Fig. 8, the component (rectangular) pulses start to separate. As will be seen, the amplitude of the received signal decreases rapidly with observation angle off broadside. This gives an effective "beamwidth" in a somewhat different sense than that derived for conventional sinusoidal signals, but nevertheless it is indicative of array directivity. Peak voltage is confined to a cap that narrows in width but does not decrease until an end-component pulse shifts a full pulse width relative to the component pulse at the other end. This occurs for ϕ determined by

$$(N-1)\, d \sin \phi = c\tau' \ . \tag{18}$$

Generalizing, the successive drops in peak voltage occur when

$$(N-1-j)\ d\ \sin\ \phi_{j+1}\ =\ c\tau;\ j\ =\ 0,1,2,\cdots,N-2\ , \tag{19}$$

where ϕ_1 is the first drop point.

Thus,

$$\phi_{j+1}\ =\ \sin^{-1}\ \frac{c\tau}{d\ (N-1-j)};\ j\ =\ 0,1,2,\cdots,N-2\ . \tag{20}$$

Peak voltage is given by

$$v_p\ =\ N-j\ \text{for}\ \phi_j\ <\ \phi\ <\ \phi_{j+1};\ j\ =\ 0,1,2,\cdots,N-1\ . \tag{21}$$

The 3 dB beam edge occurs when

$$v_p\ =\ \frac{N}{\sqrt{2}}\ =\ N-j'\ , \tag{22}$$

or when

$$j'\ =\ N-\ \frac{N}{\sqrt{2}}\ =\ N\left(\frac{\sqrt{2}\ -\ 1}{\sqrt{2}}\right)\ . \tag{23}$$

Use of this value of j in Eq. (20) gives the beam edge as *

$$\phi_E\ =\ \sin^{-1}\left\{\frac{c\tau'}{d\left[N\ -\ 1\ -\ N\left(\frac{\sqrt{2}\ -\ 1}{\sqrt{2}}\right)\right]}\right\} \tag{24}$$

or

$$\phi_E\ =\ \sin^{-1}\ \frac{\sqrt{2}\ c\tau'}{d\ (N-\sqrt{2})}\ . \tag{25}$$

*This assumes that the beam edge occurs exactly at the jump $j = j'$.

The beamwidth is therefore

$$\phi_B = 2\,\phi_E = 2\,\sin^{-1}\left[\frac{\sqrt{2}\,c\tau'}{d\,(N-\sqrt{2})}\right], \qquad (26)$$

$$= \frac{2\sqrt{2}\,c\tau'}{D} \quad \text{for } N>>1$$

where $D = N\,d$ = array length.

If the signal were sinusoidal at a carrier frequency f (wavelength λ), then

$$\phi_B' = \frac{\lambda}{D} = \frac{c}{fD}. \qquad (27)$$

By analogy, after setting

$$\phi_B = \phi_B', \qquad (28)$$

we have

$$\frac{2\sqrt{2}\,c\tau'}{D} = \frac{c}{fD} \qquad (29)$$

or

$$f = \frac{1}{2\sqrt{2}\,\tau'} = \frac{.35}{\tau'}. \qquad (30)$$

Thus, in terms of directivity, the array behaves as though sinusoids were being used with an equivalent frequency given, approximately, by one-third the reciprocal of the pulse (e.g., 333 MHz for a 1 ns pulse).

For rectangular pulses, Fig. 13 shows the temporal waveform for a 10-element array as it changes in 2° increments up to 10° off broadside. The amplitude is plotted in Fig. 14, verifying Eqs. (30) and (27). (Beamwidth is twice the beam-edge angle in Fig. 14.)

Figure 15 shows that rounded pulses give a narrower beamwidth for half-cosine pulses of width τ. Figure 14 plots the amplitude in this case also, showing that the beamwidth is about .57 times the beamwidth for rectangular pulses. This, in effect, changes the equivalent frequency in Eq. (30) to

$$f = \frac{.61}{\tau'} \qquad (31)$$

for cosine-shaped pulses.

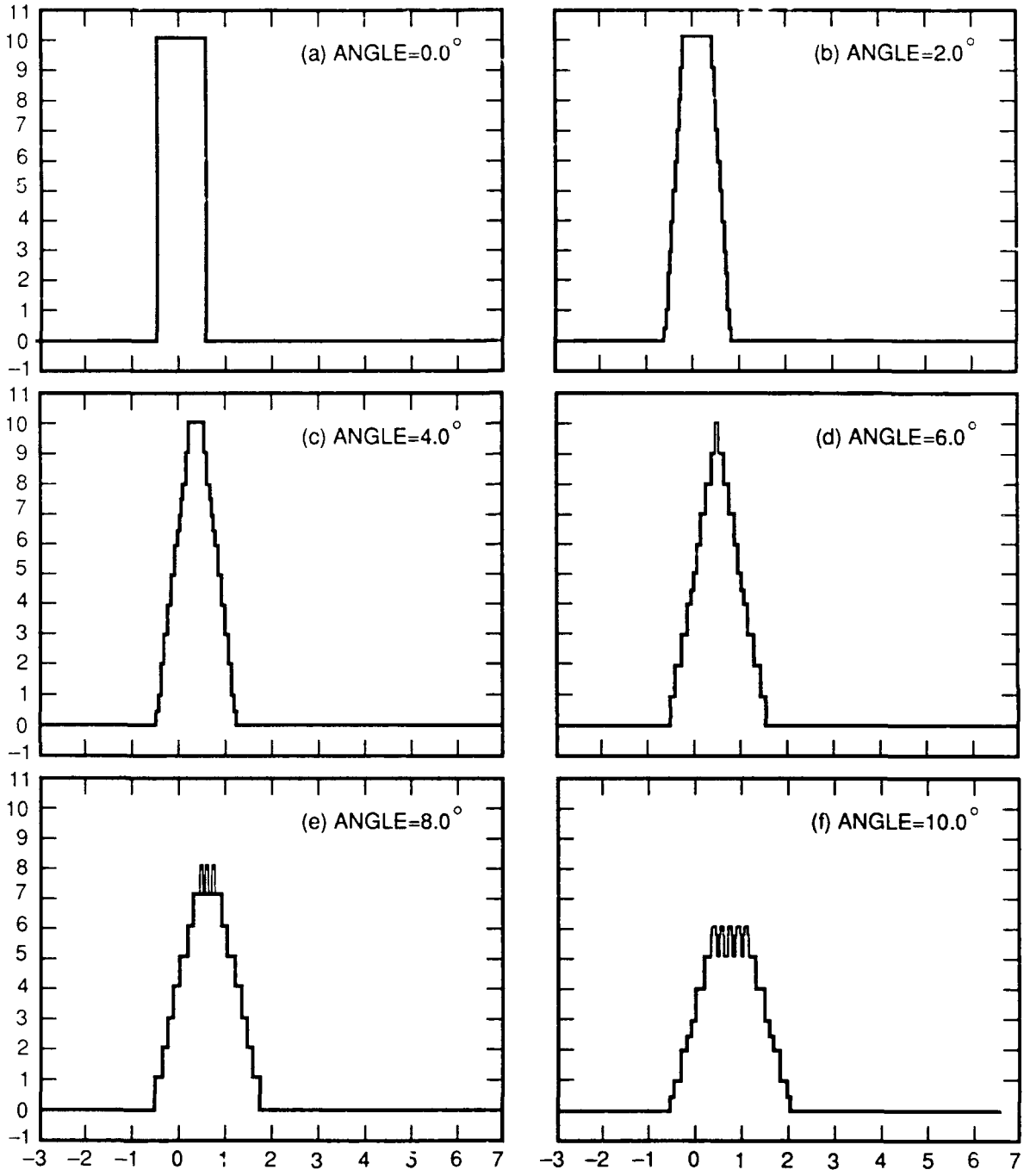

Fig. 13 — Temporal waveform for rectangular pulses, 2° increments up to 10°, $d/c\tau = 1$

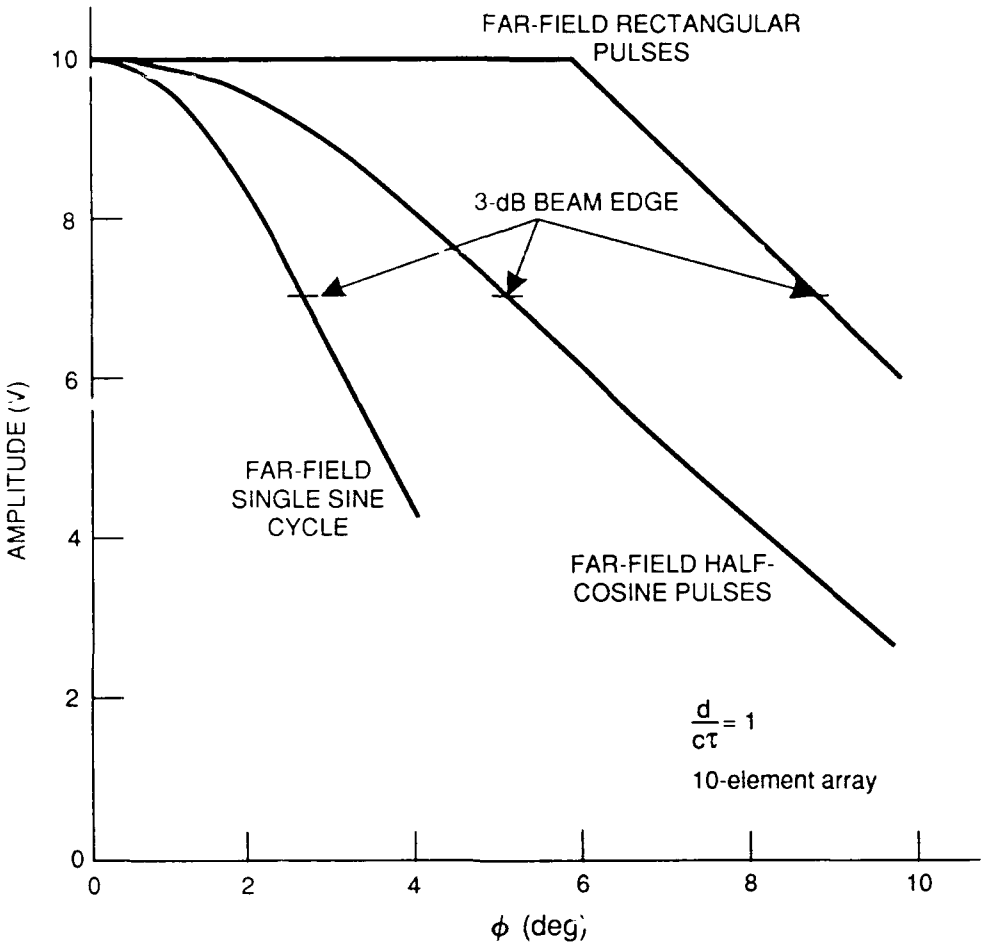

Fig. 14 — Voltage amplitude vs angle off broadside

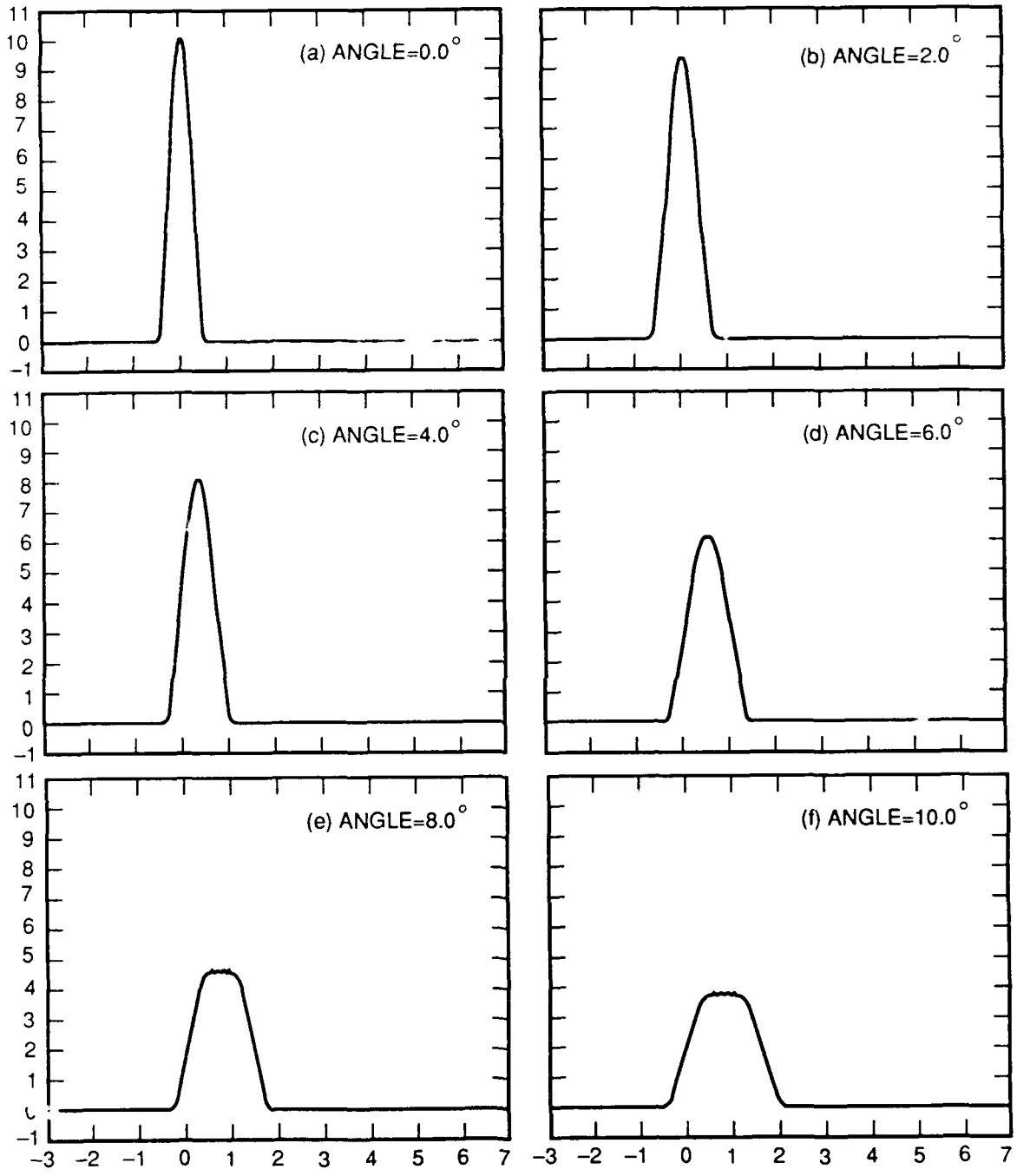

Fig. 15 — Temporal waveform for half-cosine pulses, 2° increments up to 10°, $d/c\tau = 1$

Note that in Fig. 7, however, realistic current pulses of width τ are likely to be rounded and the received derivative has a half-cycle corresponding to

$$\tau' = \tau/2. \tag{32}$$

Thus, by using Eqs. (30) and (32), the equivalent frequency is

$$f = \frac{1.2}{\tau}, \tag{33}$$

where τ is the width of the source-current pulse.

Although the previous waveforms (rectangular pulse and half cosine) are useful for determining beamwidth, they are not entirely realistic as far-field waveforms since the average value of such a signal, which is a derivative, must be zero. Figure 16 uses a far-field single-cycle sine wave (from a $\cos^2$ current pulse) and shows how it attenuates close to broadside. The results are also included in Fig. 14, where it is seen that the beamwidth is half that for the half-cosine far-field waveshape. This is as it should be, because the full sinusoid has a duration of τ comparable to the half-cosine duration.

Figure 17 shows the results for angles further off broadside. The waveform at 30° off broadside (Fig. 17(c)) results from successive cancellation of all half-cycles except for the first and last, resulting from the $\tau/2$ interelement delay. The same waveform could be obtained in an endfire mode by using an interelement spacing of $d = c\tau/2$, provided that no mutual interference effects between elements distort the results. Beyond 30°, from 45° to 90° in Fig. 17, note that the waveform appears like a 10-cycle sinusoid with varying frequency. Actually, some deviation from an exact sinusoidal shape results from the nature of the partial overlap of the component single-cycle sinusoids. At any rate, a 10-cycle sinusoid implies a nonbaseband signal with about 10% bandwidth. This is interesting considering that we started with a single baseband pulse ($\cos^2$ shape). The carrier frequency varies from $1/\tau$ at 90° to $1/.75\ \tau$ at 45° (e.g., for $\tau = 1$ ns, the frequency varies from 1 GHz at 90° to 1.33 GHz at 45°). Because the bandwidth is about 100 MHz, three "angle channels" could occur based on carrier frequency between 45° and 90°; better angle accuracy can probably be obtained by interpolation (splitting) between channels.

Generalized Expression for Beamwidth

It is useful to express beamwidth in the conventional form

$$\phi_B = \frac{\lambda_{eq}}{D} = \frac{\lambda_{eq}}{(N-1)d}, \tag{34}$$

where λ_{eq} is some "equivalent" wavelength and D is the array length.

Generally, d is conveniently expressed in terms of pulse length:

$$d = q\ c\ \tau, \tag{35}$$

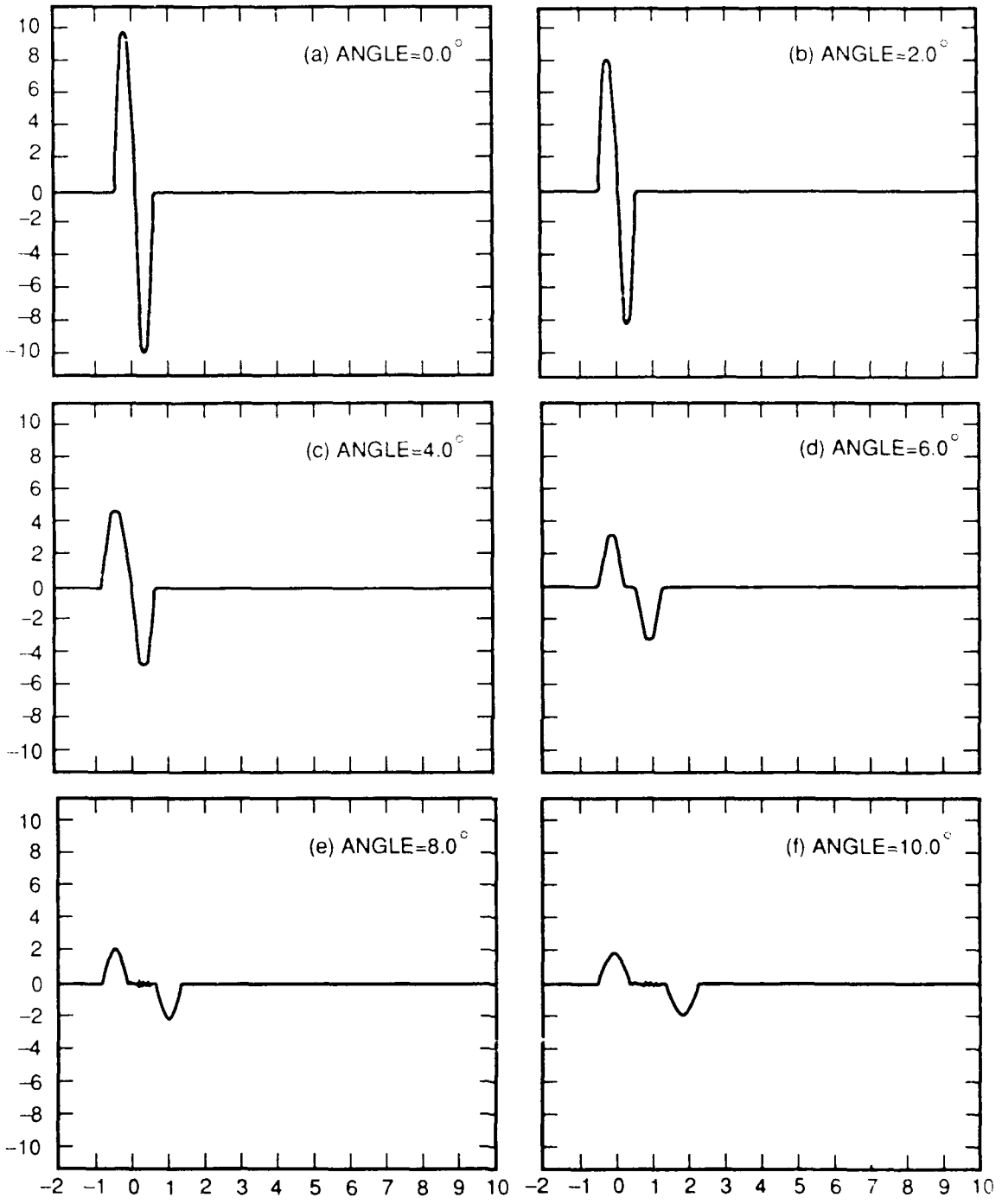

Fig. 16 — Change in single-cycle sinusoid near broadside, $d/c\tau = 1$

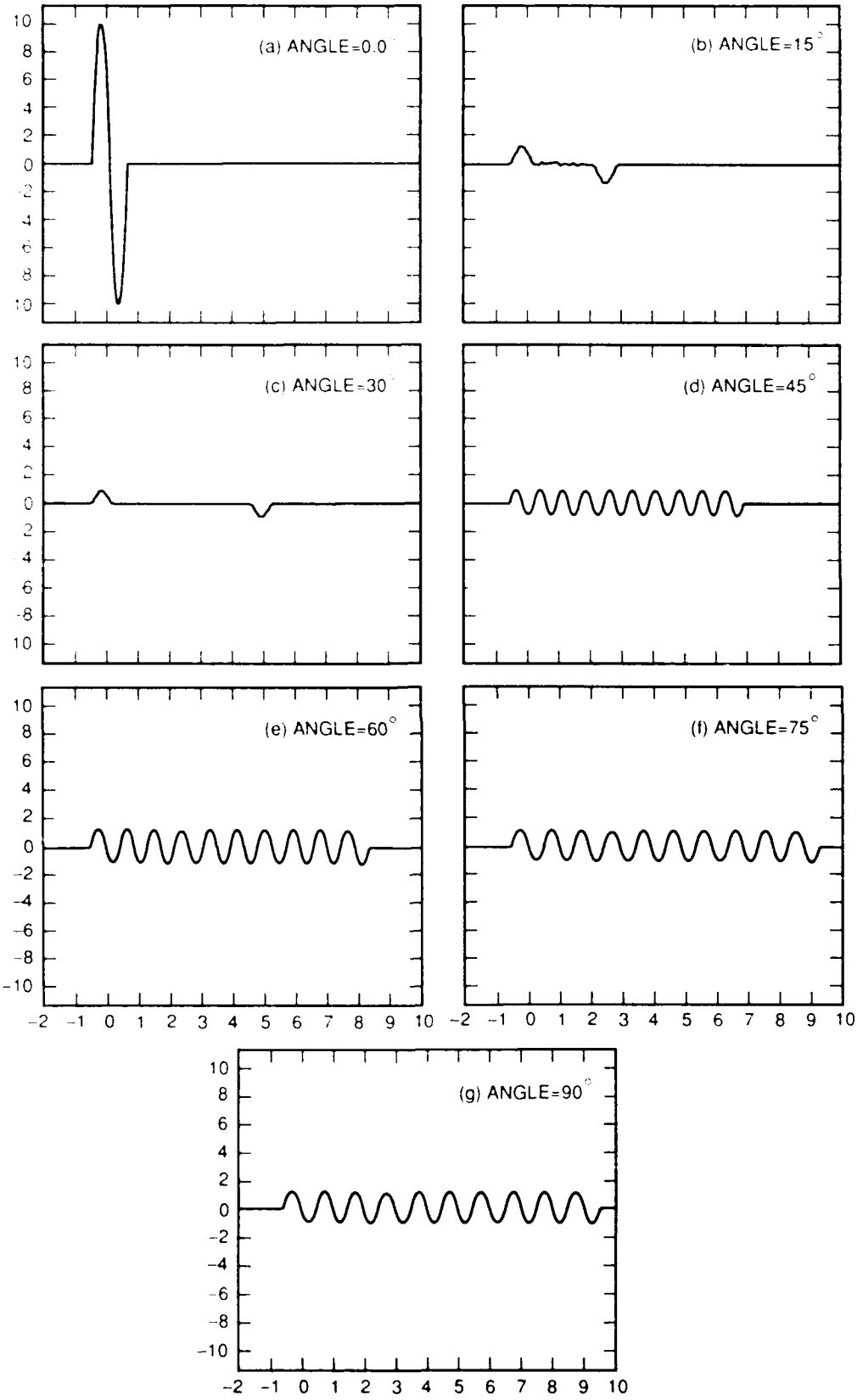

Fig. 17 – Variation of single-cycle sinusoid for larger off-broadside angles, $d/c\tau = 1$

where q is a spacing factor. Thus, Eq. (18) may be written as

$$\phi_B = \frac{\lambda_{eq}}{(N-1)\ qc\tau} = \frac{1}{(N-1)\ q\ \tau\ f_{eq}}\ , \tag{36}$$

where

$$f_{eq} = \frac{c}{\lambda_{eq}}\ . \tag{37}$$

The equivalent frequency is therefore

$$f_{eq} = \frac{1}{(N-1)q\tau\phi_B} = \frac{p}{\tau}\ , \tag{38}$$

where

$$p = \frac{1}{(N-1)q\phi_B}\ . \tag{39}$$

Summarizing the above, the conventional Eq. (34) can be used if the equivalent wavelength corresponds to an equivalent frequency given by Eq. (39). The beamwidth ϕ_B depends on pulse shape, as shown in Fig. 14.

As an example, let $N=10$ and $q=1$. From Fig. 14, we have:

Far-Field Pulse Shape	ϕ_B (deg)	p
Rectangular	17.8	.36
Half-cosine	10.2	.62
Single sine cycle*	5.6	1.22

For the very interesting case of the single sine cycle, the focusing effect of the array (from a peak power measure) is comparable to that of a conventional sinusoidal array having a monochromatic frequency equal to approximately the reciprocal of the original pulse width.

Energy Definition

We have considered beamwidth with respect to a peak voltage/power definition. This definition would be appropriate when dealing with a wideband receiver matched to a pulsewidth that would, in fact, pass the received waveshapes without distortion. However, signal-bandwidth matching to improve the

*Half sine cycle is $\tau/2$, arising from derivative of cosine on a pedestal ($\cos^2$) original pulse shape.

signal-to-noise ratio would be missing. If we were to attempt such a bandwidth match at various or all angles, detectability would depend on signal energy in the North-filter (or matched-filter) sense. In this case, a beamwidth defined in terms of energy would be more meaningful than one defined in terms of voltage/power.

For small angles off broadside, Fig. 18 shows the drop in energy E when using the waveshape class of Fig. 17: $E = \int v^2(t)dt$. The 3 dB beamwidth is approximately 5.6°, which is close to that obtained in Fig. 14 when using the peak power for the far-field single sine cycle.

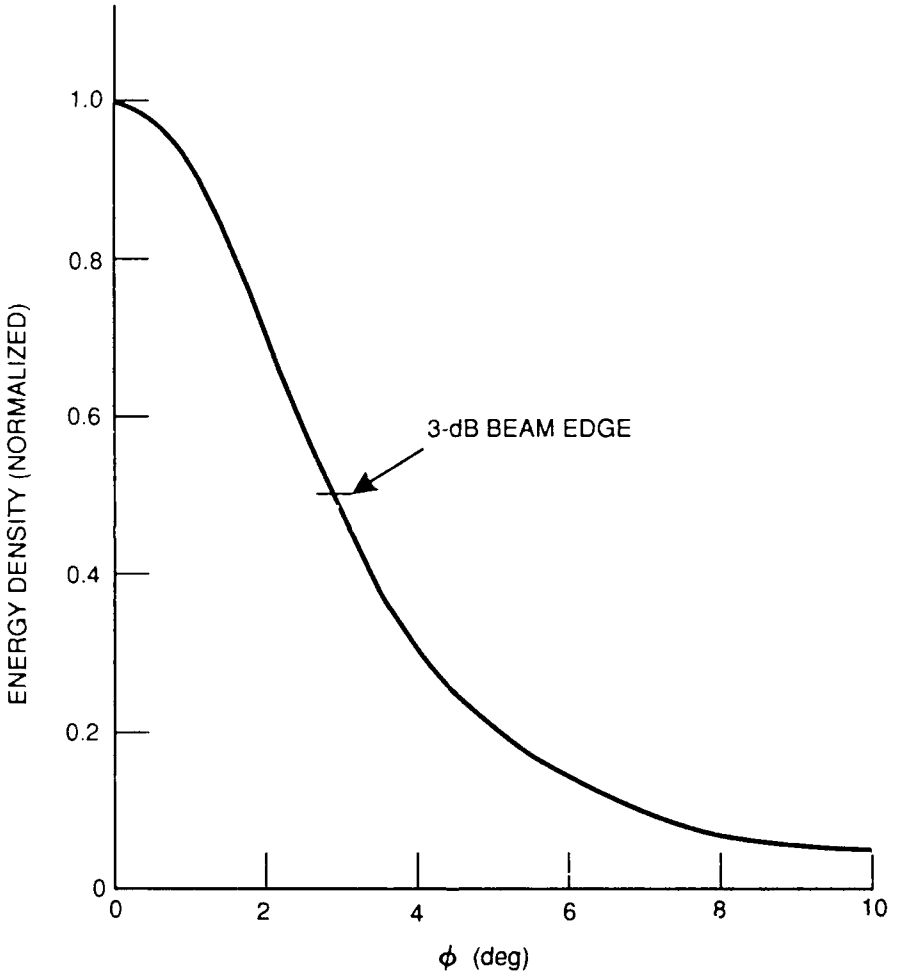

Fig. 18 — Energy variation for small angles off broadside

Note that because waveshape changes with angle, a receiver matched to the waveform in the broadside direction will become mismatched off broadside, so beamwidth will appear even smaller than that indicated in Fig. 18 in this type of implementation.

Figure 19 shows the energy variation for larger angles off boresight. The figure shows that the far-out "sidelobes" are down 10 dB for this 10-element array. This is as expected because the on-broadside waveform is of relative voltage magnitude N and duration τ, whereas the far-out waveform is of relative voltage magnitude unity and duration $N\tau$ for this interelement spacing of $d = c\,\tau$, where N is the number of array elements.

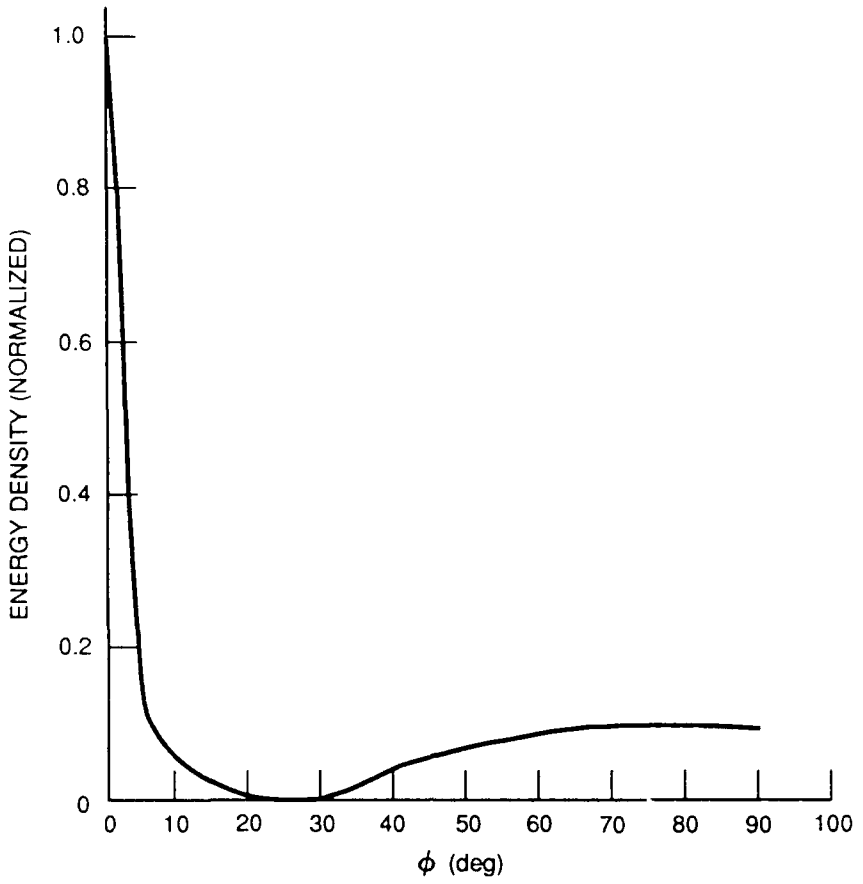

Fig. 19 — Energy variation for large angles off broadside

For comparison with results here, voltage, power and energy patterns are also given in Ref. 2 for rectangular baseband pulses.

Array Gain

Consider first a conventional square array of sinusoidal radiators with M total elements, i.e., $\sqrt{M}$ elements on each side. The beamwidth is

$$\phi_B = \frac{\lambda}{D} \tag{40}$$

and the gain is

$$G = \frac{4\pi}{\phi_B^2} = \frac{2\pi D^2}{\lambda^2} \ . \tag{41}$$

With a standard interelement spacing of

$$d = \lambda/2 \ , \tag{42}$$

we have for large M

$$D = \frac{\sqrt{M}\,\lambda}{2} \ , \tag{43}$$

and therefore

$$G = \frac{4\pi D^2}{\lambda^2} = \pi M \ . \tag{44}$$

When using a $\sqrt{M} \times \sqrt{M}$ baseband array with the waveforms of Fig. 16, we have a 3 dB beamwidth of approximately

$$\phi_B{}' = \frac{c\tau}{D} \ , \tag{45}$$

by using Eqs. (27) and (33). Analogous to Eq. (41) we have

$$G = \frac{4\pi}{\phi_B{}'^2} = \frac{4\pi D^2}{c^2\tau^2} \ . \tag{46}$$

When using

$$D = \sqrt{M} \cdot d = \sqrt{M} \cdot c\tau \ , \tag{47}$$

Eq. (46) becomes

$$G = 4\,\pi M \ . \tag{48}$$

This gives a gain four times that of the conventional array as expressed in Eq. (44). This can be explained as follows. Equation (40) was assumed to hold for both sinusoidal arrays and a baseband array, and we determined a pseudofrequency and pseudowavelength for the baseband array such that Eq. (40) applied. If we now set Eq. (40) equal to Eq. (45) to equalize the two beamwidths (and gains), then we must have

$$c\tau = \lambda \ . \tag{49}$$

But $c\tau = d$ is the interelement spacing of the baseband array that is here dictated as λ, whereas it is $\lambda/2$ for the sinusoidal array. Therefore, our baseband array is twice as large in both dimensions, and our beamwidth is half as large in both directions.

We are thus getting the correct gain and beamwidth based on physical dimensions, but Eq. (48) differs from Eq. (44) because our baseband elements are spaced further apart by a factor of two to provide the larger array with narrower beamwidths and higher gain.

If we reduce the size of our impulse array by a factor of two in each dimension and keep the same interelement spacing, we get the same beamwidth and gain as the sinusoidal array with one-fourth of the elements. This results from the larger interelement spacing that can be tolerated because grating lobes are not a problem.

On the other hand, if we reduce the interelement spacing to $d = c\tau/2$, we do not save any elements for the same beamwidth and gain as a sinusoidal array of equal size. In this sense, a spacing of $d = c\tau/2$ is analogous to $\lambda/2$ spacing in a sinusoidal array. However, now the endfire waveform is that of Fig. 17(c), and we have a very low "sidelobe" antenna in terms of energy, as seen in Fig. 19 for the range of angles from 0° to 30° that would be expanded to the range of 0° to 90°.

4. SUMMARY

The analyses presented here indicate that a baseband impulse-current element in free space will propagate pulses such that, at long ranges, the derivative of the pulse is received. This is also true in the presence of an absorbing back plane.

With a reflecting back plane, no interaction occurs as long as the plane is separated from the element by

$$\ell > \frac{\tau}{2c} , \tag{50}$$

where τ is the pulsewidth. In this case, the generated and reflected waveforms propagate sequentially with a polarity reversal in the backplane echo.

For rounded current pulse shapes at the source element such as a $\cos^2$-shaped pulse (equivalent to a full cosine on a pedestal), the derivative received waveform is a single sinusoidal cycle with a carrier frequency of

$$f = \frac{1}{\tau} \tag{51}$$

and 100% 3 dB bandwidth.

An array of such elements, with or without a reflecting back plane, has a beamwidth that can be calculated from the standard monochromatic formula

$$\phi_B = \frac{\lambda_{eq}}{D} , \tag{52}$$

where

$$\lambda = \text{monochromatic wavelength}$$
$$D = \text{aperture width,} \tag{53}$$
$$\text{with } \lambda_{eq} = \frac{c}{f_{eq}}$$

which corresponds to an equivalent frequency

$$f_{eq} = \frac{1}{\tau} . \tag{54}$$

In such an array with interelement spacing $c\tau$, as an observer moves off the broadside direction, the composite received signal from all elements changes shape radically. These signal shapes vary from a single sinusoidal cycle (100% bandwidth) to a coherent train of N contiguous sinusoidal cycles ($100/N\%$ bandwidth) in the endfire position. Use of this conclusion could lead to simpler ways of generating a conventional sinusoidal pulse.

5. ACKNOWLEDGMENT

The contributions of Kevin Luc are gratefully acknowledged in providing simulation computer plots.

REFERENCES

1. R. M. Morey, "Geophysical Surveying System Employing Electromagnetic Impulses," U.S. Patent 3,806,795, 1974.

2. P. Van Etten, "The Present Technology of Impulse Radars," International Conference, Radar-77 Oct. 25-28, 1977, organized by the Electronics Division of the Institution of Electrical Engineers, Savoy Place, London WC2, pp. 535-539. (Extensive bibliography given in paper. Also see Tri-Service Symp. papers presented by Rome Air Development Center, late 1960s and early 1970s.)

3. C. W. Harrison, Jr. and C. S. Williams, Jr., "Transients in Wide-Angle Conical Antennas," *IEEE Trans. Antennas Propag.*, **AP-13**(2), 236-246 (1965).

4. D. M. Parkes and P. D. Smith, "Transient Field Generation and Measurement," *Royal Sig. Radar Estab. Res. Rev.*, Malvern, UK (1985).

5. C. L. Bennett and G. F. Ross, "Time-Domain Electromagnetics and Its Applications," *Proc. IEEE*, **66**(3), 299-318 (1978).

6. G. F. Ross, "Balanced Radiation System," U.S. Patent 3,659,203, 1972.

7. Norfolk Ship Systems Inc. (NSSI), private communication, 1987.

8. S. Ramo and J. R. Whinnery, *Fields and Waves in Modern Radio* (John Wiley & Sons, Inc., New York, 1944).